BMC Cancer

RESEARCH

Open Access

Biparametric MRI-based radiomics for prediction of clinically significant prostate cancer of PI-RADS category 3 lesions

Feng Lu[1,3†], Yanjun Zhao[1†], Zhongjuan Wang[1] and Ninghan Feng[2,3*]

Abstract

Purpose We aimed to investigate the diagnostic performance of biparametric MRI (bpMRI)-based radiomics in differentiating clinically significant prostate cancer (csPCa) among lesions categorized as Prostate Imaging Reporting and Data System (PI-RADS) score 3.

Method Between September 2020 and October 2023, a total of 233 patients with PI-RADS category 3 lesions were identified, which were divided into training cohort ($n=160$) and validation cohort ($n=73$). Radiomics features were extracted from T2-weighted imaging (T2) and diffusion-weighted imaging (DWI) for csPCa prediction. The least absolute shrinkage and selection operator (LASSO) regression algorithm was used to select the most useful radiomics features. Diagnostic performance was compared using the area under the receiver operating characteristic (ROC) curve (AUC).

Results 34 robust radiomics features (incorporating 12 features from T2 and 22 features from DWI) were selected to construct the final radiomics signature. In the training group, the AUCs for prostate-specific antigen density (PSAD), radiomics, and combination were 0.658 (95% CI 0.550–0.766), 0.858 (95% CI 0.779–0.936), and 0.887 (95% CI 0.814–0.959), respectively, in the validation group were 0.690 (95% CI 0.524–0.855), 0.810 (95% CI 0.682–0.937), and 0.856 (95% CI 0.750–0.962). The combination model integrating radiomics and PSAD showed a significant improvement in diagnostic performance as compared to using these two parameters alone either in the training group ($P<0.001$ and $P=0.024$) or in the validation group ($P=0.024$ and $P=0.048$).

Conclusion BpMRI-based radiomics had high diagnostic performance in predicting csPCa among PI-RADS 3 lesions, and combining it with PSAD could further improve the overall accuracy.

Keywords BpMRI, Prostate cancer, PI-RADS, Radiomics, Diagnostic performance

†Feng Lu and Yanjun Zhao contributed equally to this work.

*Correspondence:
Ninghan Feng
ninghan__feng@126.com
[1]Department of Radiology, Jiangnan University Medical Center, Wuxi, China
[2]Department of Urological Surgical, Jiangnan University Medical Center, Wuxi, China
[3]Wuxi School of Medicine, Jiangnan University, Wuxi, China

Introduction

Prostate Cancer (PCa) is the second most common cancer among men worldwide, and one of the leading causes of cancer-associated death in men [1]. It is estimated that 1.2 million new cases of PCa are diagnosed every year and 350,000 die of it [2]. In the past two decades, MRI has been established as the most effective imaging modality in the detection, diagnosis, and management of PCa [3–5]. The mpMRI-based PI-RADS demonstrated high diagnostic performance and has been widely used for risk stratification of PCa [6–8]. Nevertheless, PI-RADS category 3 lesions pose a clinical dilemma, as physicians must balance the need for cancer detection with the goal of avoiding unnecessary biopsies. The PI-RADS recommends lesions categorized as ≥ 3 referred to biopsy; however, it is estimated that only 36% and 18.5% of these indeterminate lesions are PCa and csPCa, resulting in a great number of unnecessary biopsies [9]. Unnecessary biopsies and overtreatment may lead to complications such as infection or sepsis. Thus, it is needed to improve the diagnostic accuracy for these equivocal lesions, thereby reducing unnecessary biopsies.

Over the last decade, radiomics has emerged as a promising approach to detecting various cancers. The rationale behind radiomics is that medical images contain more information than can be visually discerned by experienced radiologists, which facilitate diagnosis, risk stratification, and predicting therapeutic outcomes. Previous studies have underscored radiomics' potential in PCa detection, aggressiveness assessment, and survival analysis [10–12]. Most of these studies have, however, focused on quantitative features extracted from full sequences of mpMRI including T2, dynamic contrast-enhanced (DCE) images, DWI, and apparent diffusion coefficient (ADC) [6, 13]. Notably, several studies have demonstrated that DCE merely plays a secondary role in the transition zone (TZ) and may be unnecessary for peripheral zone (PZ) lesions [14–16]. As a result, the concept of biparametric MRI, which excludes DCE, has gained substantial attention. This approach significantly reduces image acquisition time and examination costs while maintaining comparable diagnostic accuracy compared to mpMRI [17–20]. In this study, we aimed to evaluate the diagnostic accuracy of bpMRI-based radiomics for the detection of csPCa among PI-RADS score 3 lesions. In addition, the performance of a nomogram combining radiomics and PSAD has been investigated.

Materials and methods

Patient selection

This retrospective study was approved by the institutional review board (IRB) of Wuxi No. 2 People's Hospital, and the requirement for informed consent was waived. Between September 2020 and October 2023, patients who underwent bpMRI examination and subsequently MRI/US fusion biopsy were queried from our institution's electric medical records. We identified lesions that scored as category 3 based on PI-RADS v2.1 guideline, which were assessed by two dedicated radiologists (with 5 years and 6 years of experience in urology radiology) independently, who were blinded to pathological results, with discrepancies resolved through discussion.

According to the inclusion criteria, 279 individuals were identified initially. However, 46 patients were excluded because of the following reasons: (1) history of biopsy or treatment ($n = 16$); (2) images were fuzzy or with artifacts ($n = 21$); and (3) insufficient clinical data ($n = 9$). Finally, a total of 233 patients (mean age 70.12 ± 7.77 years; median PSA 8.32, interquartile range [IQR] 6.13–10.60 ng/mL) were included in the current study, of which 160 were randomized to the training cohort and 73 were randomized to the validation cohort. Figure 1 shows the details of the patient selection diagram.

MRI acquisition and interpretation

All prostate MRI examinations were performed on a 3.0T scanner (MAGNETOM Skyra, Siemens AG), and a pelvic 32-channel phased array coil was used. MRI protocols included T2 and DWI, details on image acquisition parameters are described in Table 1.

Prostate biopsy procedure

Lesions suspicious of PCa underwent MRI/US fusion biopsy within four weeks after MRI examination. The fusion biopsy was performed by a urologist with 12 years of experience, using a color Doppler ultrasound device, with a real-time virtual sonography imaging fusion system. Identified lesions were annotated on T2 images by the radiologists and segmented with real-time transrectal ultrasound. For each lesion, at least two fusion-guided targeted cores (axial and sagittal planes) were obtained. An expert genitourinary pathologist evaluated the biopsy specimens and assigned each lesion a Gleason score (GS), who has an experience of 16 years and was blinded to the MRI findings. Each lesion that was suspected for PCa was designated to the corresponding grade group according to the International Society of Urological Pathology (ISUP). The biopsy results were evaluated to determine the location and GS of an index tumor with the highest GS. csPCa was defined as GS ≥ 7 (ISUP ≥ 2). The volume of the prostate was determined with the ellipsoid volume formula and the tumor size was decided on the base of T2 images.

Feature extraction and radiomics analysis

Two radiologists manually segmented images from two MRI sequences of axial T2 and DWI (3D slicer,

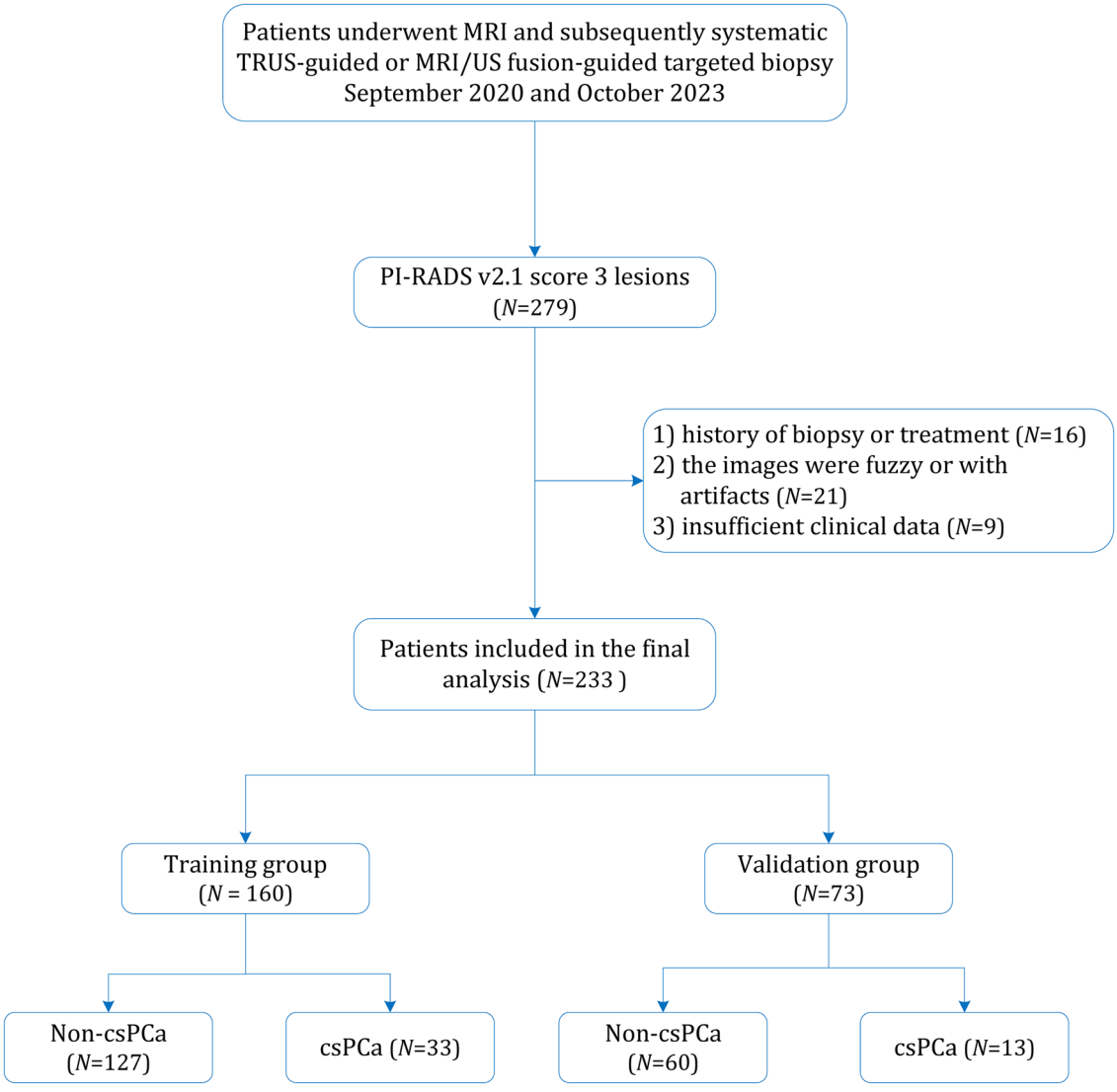

Fig. 1 Flowchart of the study population with the exclusion criteria. csPCa, clinically significant prostate cancer

Table 1 MRI parameters

Parameter	Sequence			
	T1WI (axial)	T2WI (axial)	T2WI (sagittal)	DWI
Field of view (mm)	300×300	230×230	230×230	320×224
Acquisition matrix	256×205	320×224	320×256	192×192
Repetition time (ms)	744	4400	3800	6570
Echo time (ms)	13	96	117	88
Section thickness, no gaps (mm)	3.0	3.0	3.0	3.0
Acquisition time	1 m 37s	2 m 49s	2 m 24s	4 m 56s

Abbreviations: DCE, dynamic contrast enhanced imaging; DWI, diffusion weighted imaging; T1WI, T1-weighted imaging; T2WI, T2-weighted imaging. DWI performed with ***b*** values of 0, 100, and 1000s/mm^2

version 5.0.3), and radiomics features with suspected PCa were extracted from regions of interest (ROI) with PyRadiomics (version 3.1.0). Extracted features including first-order, shape, and texture features encompassing Gray-Level Cooccurrence Matrix (GLCM), Gray-Level Dependence Matrix (GLDM), Gray-Level Run Length Matrix (GLRLM), Gray-Level Size Zone Matrix (GLSZM), and Neighboring Gray-Tone Difference Matrix (NGTDM). Additionally, two kinds of filters (Laplacian of Gaussian and wavelet) that derived from original images were used to extract additional features. The LASSO regression algorithm was used to select the most useful radiomics features. The most important radiomics features derived from the LASSO classifier were used to develop radiomics signature (Radscore), with 10-fold cross-validation on the training set. The Radscore was calculated via a linear combination of selected features

weighted by their respective coefficients with the following formula:

Radscore = intercept + $\beta_i \times X_i$. (β, the coefficient of each radiomics feature; X, nonzero coefficient radiomics features; i, the sequence number of features).

The value of each nonzero coefficient radiomics feature are presented in Table S1.

Statistical analysis

Kolmogorov–Smirnov test was used to examine the normal distribution of data. Descriptive statistics of continuous variables are shown as mean ± standard deviation (SD) for normally distributed or median (interquartile range, IQR) for non-normally distributed. Comparisons between the two groups were evaluated using Mann-Whitney's U test (non-normally distributed variables) and independent *t*-test (normally distributed variables). Because the sample of csPCa was smaller than non-csPCa, we used the Synthetic Minority Oversampling Technique (SMOTE) to oversample the minority class. Here, the minority class is over-sampled by generating synthetic examples along the line segments connecting each minority class sample to any or all its k nearest minority class neighbors. This oversampling method randomly generates new instances of the minority class to balance the dataset. Notably, the SMOTE method was not applied to the validation group. Sensitivity, specificity, positive likelihood ratio (LR+), and negative likelihood ratio (LR-) were calculated to evaluate the diagnostic accuracy. The overall performance was assessed with the AUC and differences between models were compared with DeLong's test [21]. All analysis was performed with STATA 16.1, R 4.3.2, and Python 3.7. ***P*** values ≤ 0.05 were considered statistically significant. Decision curve analysis (DCA) was conducted to assess the clinical usefulness and benefits of the combined model at different threshold probabilities [22]. A calibration curve was plotted to explore the predictive accuracy of radiomics and the combined nomogram [23].

Results

Patient characteristics

The demographic characteristics are summarized in Table 2. At the final fusion MRI/US fusion biopsy, the cancer detection rate was 33/160 (20.63%) in the training group and 13/73 (17.81%) in the validation group. The Kolmogorov-Smirnov test demonstrated that only variable of age was distributed normally ($P = 0.12$ and $P = 0.19$), whereas the PSA level and PSAD were unnormal ($P < 0.001$). There was no significant difference between the training group and validation group in terms of age, PSA level, and PSAD, with a P value of 0.51–0.90.

Diagnostic performance of using PSAD

In the training cohort, PSAD yielded an AUC of 0.658 (95% CI 0.550–0.766). The optimal cutoff value for PSAD was 0.21 ng/ml/ml, where the sensitivity and specificity were 36.4% (95% CI 20.4%-54.9%) and 81.9% (95% CI 74.1%-88.2%), respectively. Comparable diagnostic performance was observed in the validation group, with an AUC of 0.690 (95% CI 0.524–0.855). At a threshold of 0.18 ng/ml/ml, the sensitivity and specificity were 46.2% (95% CI 19.2%-74.9%) and 68.3% (95% CI 54.8%-79.7%), respectively.

Diagnostic performance of radiomics

A total of 1239 features were extracted from MRI images initially, of which 618 were from the T2 sequence and 621 were from DWI. Following LASSO regression analysis, 34 robust radiomics features (incorporating 12 features

Table 2 Characteristics of patients

Variable	Training ($n = 160$)			Validation ($n = 73$)		
	csPCa ($n = 33$)	Non-csPCa ($n = 127$)*	Total	csPCa ($n = 13$)	Non-csPCa ($n = 60$)*	Total
Age (Years, mean ± SD)	73.94 ± 5.99	68.57 ± 7.68	69.68 ± 7.66	76.15 ± 5.29	69.97 ± 8.06	71.07 ± 7.98
PSA (ng/mL, median [IQR])	9.38 (6.71–18.37)	7.95 (5.60–9.48)	8.10 (5.94–9.95)	9.38 (8.73–30.96)	8.43 (6.12–14.85)	8.73 (6.30-14.92)
PSAD (ng/mL/mL, median [IQR])	0.15 (0.12–0.28)	0.12 (0.09–0.17)	0.13 (0.10–0.19)	0.17 (0.13–0.33)	0.13 (0.10–0.24)	0.13 (0.10–0.24)
Gleason score						
< 3 + 3	113			48		
3 + 3	14			9		
3 + 4	20			5		
4 + 3	8			4		
4 + 4	2			3		
> 4 + 4	3			1		

Abbreviations: csPCa, clinically significant prostate cancer; IQR, interquartile range; PI-RADS, Prostate Imaging Reporting and Data System, version 2.1; PSA, prostate-specific antigen; PSAD, prostate-specific antigen density; SD, standard deviation

Note:* Including benign prostatic hyperplasia

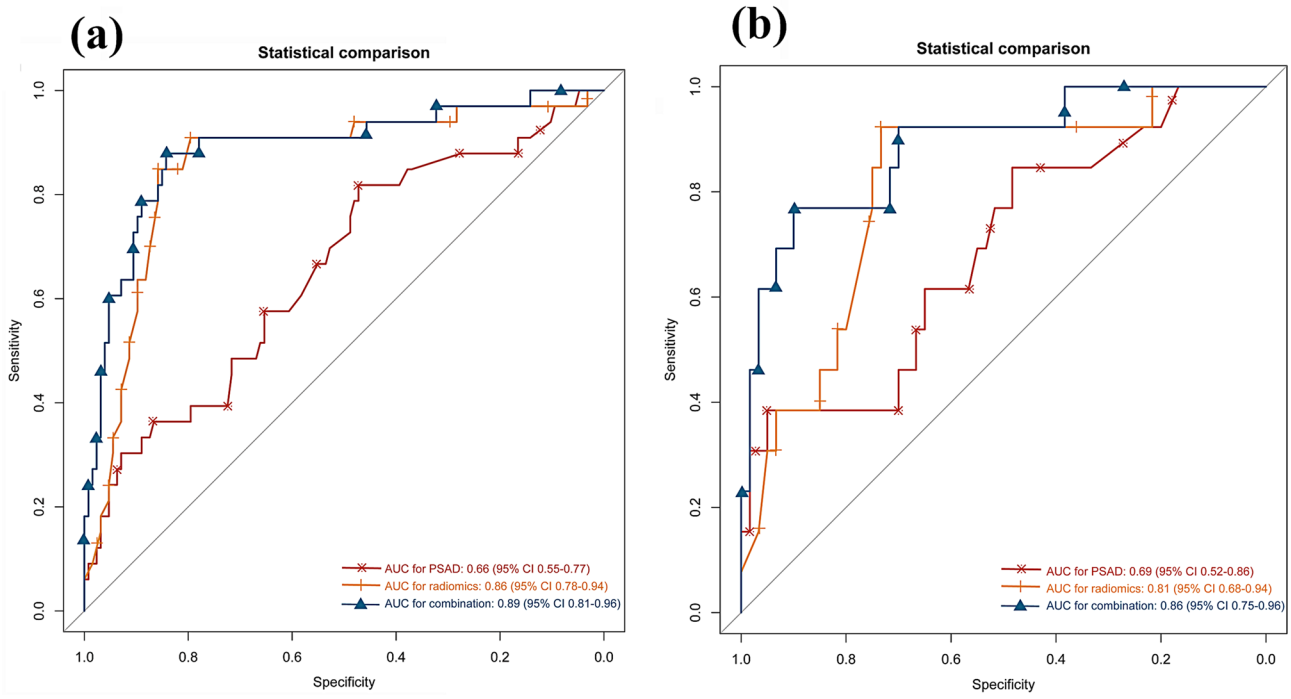

Fig. 2 ROC analysis for PSAD, radiomics, and the combination of PSAD and radiomics for prediction of clinically significant prostate cancer. **A**, training group; **B**, validation group. PSAD, prostate-specific antigen density

Table 3 Diagnostic performance

Indicator	Sensitivity (95% CI)	Specificity (95% CI)	LR+ (95% CI)	LR- (95% CI)	AUC (95% CI)	*P* for AUC[a]
Training Cohort						
PSAD ≥ 0.21	36.4% (20.4-54.9%)	81.9% (74.1-88.2%)	2.01 (1.12–3.60)	0.78 (0.59–1.02)	0.658 (0.550–0.766)	< 0.001
Radscore	84.8% (68.1-94.9%)	85.0% (77.6-90.7%)	5.67 (3.66–8.80)	0.18 (0.08–0.40)	0.858 (0.779–0.936)	0.030
PSAD + Radscore	84.8% (68.1-94.9%)	88.2% (81.3-93.2%)	7.18 (4.37–11.80)	0.17 (0.076–0.37)	0.887 (0.814–0.959)	/
Validation Cohort						
PSAD ≥ 0.18	46.2% (19.2-74.9%)	68.3% (54.8-79.7%)	1.46 (0.73–2.92)	0.79 (0.46–1.34)	0.690 (0.524–0.855)	0.024
Radscore	76.9% (46.2-95%)	91.7% (81.6-97.2%)	9.23 (3.79–22.5)	0.25 (0.09–0.68)	0.810 (0.682–0.937)	0.048
PSAD + Radscore	92.3% (64-99.8%)	76.7% (64.0-86.6%)	3.96 (2.44–6.42)	0.10 (0.02–0.66)	0.856 (0.750–0.962)	/

Abbreviations: AUC, area under the receiver operating characteristic curve; CI, confidence interval; LR+, positive likelihood ratio; LR-, negative likelihood ratio; PI-RADS, Prostate Imaging Reporting and Data System; PPV, positive predictive value; PSAD, prostate-specific antigen density; Radscore, radiomic score

Note: [a] compared with PSAD + Radscore

from T2 and 22 features from DWI) with non-zero coefficients were selected to construct the final radiomics signature. Specifically, this included 4 shape features, 7 GLRLM features, 13 first-order features, 1 NGTDM feature, 1 GLSZM, 5 GLCM features, and 3 GLDM features. No significant difference in radiomics score was observed between the training and validation groups ($P = 0.23$); however, for the csPCa and non-csPCa subgroup, a significant difference was observed in the training set (median 1.65 vs. − 2.38, $P < 0.001$) and confirmed in the validation set (median 1.39 vs. -2.07, $P = 0.001$).

In the training cohort, the calculated AUC for radiomics was 0.858 (95% CI 0.779–0.936), significantly higher than PSAD ($P < 0.001$), with sensitivity and specificity of 84.8% (95% CI 68.1%-94.9%) and 85.0% (95% CI 77.6%-90.7%), respectively. When combining radiomics and PSAD, the diagnostic performance was improved substantially, yielding an AUC of 0.887 (95% CI 0.814–0.959, $P = 0.03$). The ROC analysis for PSAD, radiomics, and their combination is demonstrated in Fig. 2 and Table 3. In the validation data set, the AUC for radiomics was 0.810 (95% CI 0.682–0.937). The AUC for the combination of radiomics and PSAD was 0.856 (95% CI 0.750–0.962), indicating a significant improvement in csPCa prediction as compared with using these two variables alone, with ***P*** values of 0.024 and 0.048. The decision curve analysis is illustrated in Fig. 3, demonstrating the clinical utility of the predictive model in both the training group and validation group. The calibration curves showed good concordance between the predicted

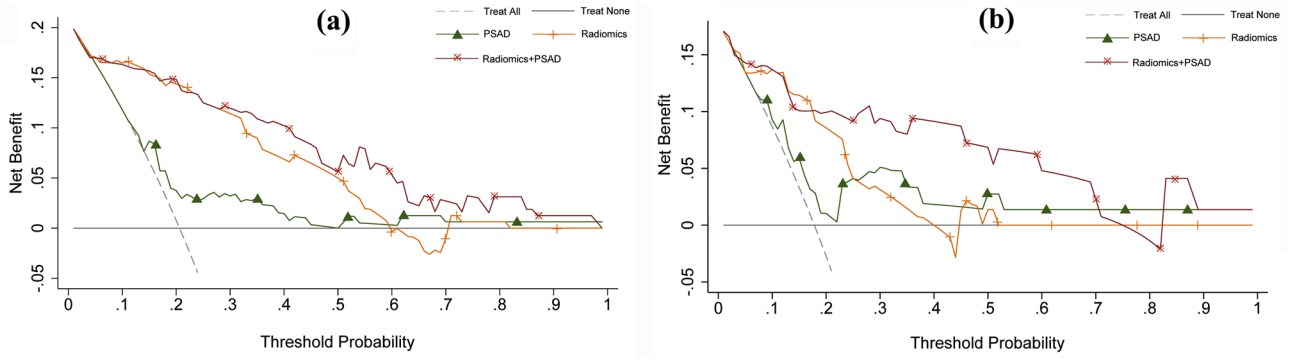

Fig. 3 Decision curves analyses for PI-RADS, radiomics, and the combination of PI-RADS and radiomics for prediction of clinically significant prostate cancer. **A**, training group; **B**, validation group. PSAD, prostate-specific antigen density

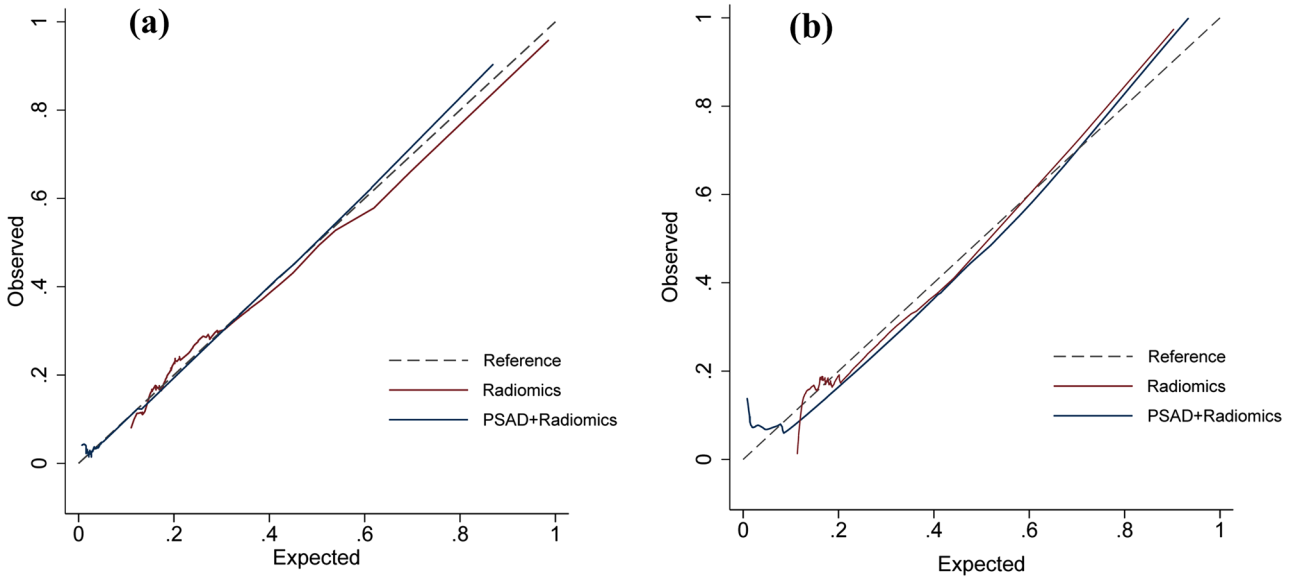

Fig. 4 Calibration curves. **A**, training group; **B**, validation group. PSAD, prostate-specific antigen density

probabilities of csPCa and the observed outcomes, which are demonstrated in Fig. 4.

Discussion

In this study, we assessed bpMRI-based radiomics for predicting csPCa in lesions classified as PI-RADS category 3. Our analysis demonstrated that radiomics achieved higher diagnostic accuracy, with an AUC of 0.858 in the training group and 0.810 in the validation group. Furthermore, in the training group combination of Radscore and PSAD resulted in a substantial improvement compared to using radiomics alone. Previous studies have shown the promising performance of using MRI-based radiomics for the prediction of csPCa in PI-RADS category 3 lesions, typically extracting features from mpMRI sequences, including T2, ADC, DWI, and DCE, with AUCs ranging from 0.75 to 0.86 [24–28]. Jin et al. used bpMRI-based radiomics for predicting PI-RADS category 3 lesions, in which the calculated AUC were 0.90 in the training group and 0.88 in the validation group [29].

In an earlier study involving 160 PI-RADS category 3 lesions, with features extracted from T2 and ADC, the generated AUCs were 0.547 and 0.684 [30]. Among previous studies, the selected features varied widely, ranging from 3 to 149. In this study, we included 40 features (12 from the T2 sequence and 22 from the DWI sequence) using the LASSO regression algorithm. Regarding the final radiomics model, some studies have used support vector machine, K-nearest neighbors, or random forest; in contrast, we employed the logistic regression algorithm in this study. At present, however, there is no conclusive evidence indicating which machine learning method is optimal. Compared with previous studies, we included more patients as compared with these two earlier studies. However, it is unfeasible to perform a comparison between studies due to discrepancies in

radiologists' experience, segmentation, and machine learning algorithms.

In the current study, we only used features extracted from T2WI and DWI. T2WI provides excellent soft tissue contrast, allowing for detailed visualization of prostate anatomy. It is especially useful for identifying structural abnormalities within the prostate. On the other hand, DWI offers insights into the cellular density of tissues by measuring the diffusion of water molecules, which tends to be restricted in cancerous tissues due to their higher cellularity [31]. These two sequences have demonstrated a negative correlation with the proportion of nuclei or cytoplasm in prostate tissue while displaying a positive correlation with the luminal space percentage [31]. As Gleason scores increase, disrupted gland architecture leads to a more disorderly and dispersed appearance of the gland lumen [12]. These histological changes manifest as specific patterns on T2WI and DWI, forming the basis for using these imaging modalities in radiomic analyses.

Our study highlighted the potential of radiomics analysis using bpMRI images of T2 and DWI to identify csPCa within PI-RADS 3 lesions. Radiomics involves extracting, measuring, and analyzing quantitative attributes from medical images to capture details beyond visual perception, assisting in lesion classification, risk assessment, and clinical decision-making. Our findings indicated that radiomics significantly outperforms PSAD in identifying csPCa in PI-RADS 3 lesions. Moreover, compared with most previous studies that focused on radiomics alone, our study demonstrated that combining radiomics with other clinical variables such as PSAD could significantly improve the overall diagnostic performance. In the current study, the imbalance of the sample (Non-csPCa vs. PCa) would reduce the performance of the classifier. To overcome the adverse impact of imbalance sample, we employed the SMOTE method, which has been proven to be an effective approach for dealing with imbalanced datasets [32].

Another issue that should be taken into consideration in radiomics analysis is segmentation, which plays an important role as it determines the accurate delineation of the ROI used for subsequent feature extraction and analysis. Despite advancements in image analysis techniques, manual contouring remains the predominant method for defining lesion volumes in radiomic studies. This approach involves radiologists manually outlining the ROI on MRI scans, which can be time-consuming and subject to variability [33]. One major limitation of manual contouring is its reliance on single image slices rather than a comprehensive 3D assessment of the entire lesion, which limits the accuracy and completeness of the volumetric characterization of lesions. Nevertheless, it is reported that features derived from automatically segmented masks exhibited slightly inferior performance when compared to manually segmented masks, which could be attributed to the potentially reduced accuracy of the auto-segmentation algorithm [33]. Moreover, the decreased effectiveness of the auto-segmentation might arise from its ability to only detect lesions in the PZ, necessitating a separate system for segmenting lesions in the TZ.

Our study has limitations that should be acknowledged. First, this is a retrospective, single-center study, which may affect the generalization of our conclusion in clinical application, and the findings need to be validated externally. Second, the classification of lesions according to PI-RADS was subjectively by radiologists, thus the results primarily depended on the radiologist's personal experience. Furthermore, ROIs were manually segmented by the radiologists rather than semi-automatic or automatic delineation, which may bring bias and be time-consuming. Finally, we did not separately analyze lesions according to the PZ and TZ anatomical zones, and future studies evaluating radiomics features classified for each zone are warranted.

Conclusions

The findings of the current study suggest that bpMRI-based radiomics had high diagnostic performance in identifying csPCa in PI-RADS category 3 lesions. Nevertheless, PSAD exhibited only moderate accuracy as an independent predictor. Notably, integrating PSAD with PI-RADS v2.1 could enhance the predictive accuracy for csPCa. These findings underscore the potential of combining radiomics and clinical indicators in prostate cancer diagnostics. To further substantiate our results, there is a need for prospective, multicenter studies to provide external validation.

Supplementary Information

The online version contains supplementary material available at https://doi.org/10.1186/s12885-025-14022-1.

Supplementary Material 1

Acknowledgements
Not applicable.

Author contributions
L.F. and Z.Y.J.: conceptualization and writing; Z.Y.J. and W.Z.J.: software and statistical analysis. L.F. and W.Z.J.: data collection and writing—original draft; F.N.H.: Writing—review, project development and supervision.

Funding
This study is supported by "Top Talent Support Program for young and middle-aged people of Wuxi Health Committee" (No. HB2023022) and "Scientific Research Program of Wuxi Health Commission" (No. M202236).

Data availability
The data that support the findings of this study are available from the corresponding author upon reasonable request.

Declarations

Ethics approval and consent to participate
Written informed consent was waived by the Institutional Review Board.

Consent for publication
Patients' data were anonymized. Not applicable.

Competing interests
The authors declare no competing interests.

Received: 12 July 2024 / Accepted: 26 March 2025
Published online: 05 April 2025

References
1. Sung H, Ferlay J, Siegel RL, Laversanne M, Soerjomataram I, Jemal A, et al. Global cancer statistics 2020: GLOBOCAN estimates of incidence and mortality worldwide for 36 cancers in 185 countries. CA Cancer J Clin. 2021;71:209–49. https://doi.org/10.3322/caac.21660.
2. Sandhu S, Moore CM, Chiong E, Beltran H, Bristow RG, Williams SG. Prostate cancer. Lancet. 2021;398:1075–90. https://doi.org/10.1016/S0140-6736(21)00950-8.
3. Tamada T, Sone T, Higashi H, Jo Y, Yamamoto A, Kanki A, et al. Prostate cancer detection in patients with total serum Prostate-Specific antigen levels of 4–10 Ng/mL: diagnostic efficacy of Diffusion-Weighted imaging, dynamic Contrast-Enhanced MRI, and T2-Weighted imaging. AJR Am J Roentgenol. 2011;197:664–70. https://doi.org/10.2214/AJR.10.5923.
4. Vilanova JC, Barceló-Vidal C, Comet J, Boada M, Barceló J, Ferrer J, et al. Usefulness of prebiopsy multifunctional and morphologic MRI combined with Free-to-Total prostate-Specific antigen ratio in the detection of prostate cancer. Am J Roentgenol. 2011;196:W715–22. https://doi.org/10.2214/AJR.10.5700.
5. Delongchamps NB, Rouanne M, Flam T, Beuvon F, Liberatore M, Zerbib M, et al. Multiparametric magnetic resonance imaging for the detection and localization of prostate cancer: combination of T2-weighted, dynamic contrast-enhanced and diffusion-weighted imaging. Bju Int. 2011;107:1411–8. https://doi.org/10.1111/j.1464-410X.2010.09808.x.
6. Barentsz JO, Richenberg J, Clements R, Choyke P, Verma S, Villeirs G, et al. ESUR prostate MR guidelines 2012. Eur Radiol. 2012;22:746–57. https://doi.org/10.1007/s00330-011-2377-y.
7. Weinreb JC, Barentsz JO, Choyke PL, Cornud F, Haider MA, Macura KJ, et al. Eur Urol. 2016;69:16–40. PI-RADS Prostate Imaging– Reporting and Data System: 2015, Version 2.
8. Turkbey B, Rosenkrantz AB, Haider MA, Padhani AR, Villeirs G, Macura KJ, et al. Eur Urol. 2019;76:340–51. https://doi.org/10.1016/j.eururo.2019.02.033. Prostate Imaging Reporting and Data System Version 2.1: 2019 Update of Prostate Imaging Reporting and Data System Version 2.
9. Maggi M, Panebianco V, Mosca A, Salciccia S, Gentilucci A, Di Pierro G, et al. Prostate imaging reporting and data system 3 category cases at multiparametric magnetic resonance for prostate cancer: A systematic review and Meta-analysis. Eur Urol Focus. 2020;6:463–78. https://doi.org/10.1016/j.euf.2019.06.014.
10. Calimano-Ramirez LF, Virarkar MK, Hernandez M, Ozdemir S, Kumar S, Gopireddy DR, et al. MRI-based nomograms and radiomics in presurgical prediction of extraprostatic extension in prostate cancer: a systematic review. Abdom Radiol. 2023;48:2379–400. https://doi.org/10.1007/s00261-023-03924-y.
11. Chiacchio G, Castellani D, Nedbal C, De Stefano V, Brocca C, Tramanzoli P, et al. Radiomics vs radiologist in prostate cancer. Results from a systematic review. World J Urol. 2023. https://doi.org/10.1007/s00345-023-04305-2.
12. Cutaia G, La Tona G, Comelli A, Vernuccio F, Agnello F, Gagliardo C, et al. Radiomics and prostate MRI: current role and future applications. J Imaging. 2021;7:34. https://doi.org/10.3390/jimaging7020034.
13. Rosenkrantz AB, Ginocchio LA, Cornfeld D, Froemming AT, Gupta RT, Turkbey B, et al. Interobserver reproducibility of the PI-RADS version 2 lexicon: A multicenter study of six experienced prostate radiologists. Radiology. 2016;280:793–804. https://doi.org/10.1148/radiol.2016152542.
14. De Visschere P, Lumen N, Ost P, Decaestecker K, Pattyn E, Villeirs G. Dynamic contrast-enhanced imaging has limited added value over T2-weighted imaging and diffusion-weighted imaging when using PI-RADSv2 for diagnosis of clinically significant prostate cancer in patients with elevated PSA. Clin Radiol. 2017;72:23–32. https://doi.org/10.1016/j.crad.2016.09.011.
15. Greer MD, Shih JH, Lay N, Barrett T, Kayat Bittencourt L, Borofsky S, et al. Validation of the dominant sequence paradigm and role of dynamic Contrast-enhanced imaging in PI-RADS version 2. Radiology. 2017;285:859–69. https://doi.org/10.1148/radiol.2017161316.
16. Obmann VC, Pahwa S, Tabayayong W, Jiang Y, O'Connor G, Dastmalchian S, et al. Diagnostic accuracy of a rapid biparametric MRI protocol for detection of histologically proven prostate cancer. Urology. 2018;122:133–8. https://doi.org/10.1016/j.urology.2018.08.032.
17. Niu X, Chen X, Chen Z, Chen L, Li J, Peng T. Diagnostic performance of biparametric MRI for detection of prostate cancer: A systematic review and Meta-Analysis. Am J Roentgenol. 2018;211:369–78. https://doi.org/10.2214/AJR.17.18946.
18. Bass EJ, Pantovic A, Connor M, Gabe R, Padhani AR, Rockall A, et al. A systematic review and meta-analysis of the diagnostic accuracy of biparametric prostate MRI for prostate cancer in men at risk. Prostate Cancer Prostatic Dis. 2021;24:596–611. https://doi.org/10.1038/s41391-020-00298-w.
19. Cuocolo R, Verde F, Ponsiglione A, Romeo V, Petretta M, Imbriaco M, et al. Clinically significant prostate cancer detection with biparametric MRI: A systematic review and Meta-Analysis. Am J Roentgenol. 2021;216:608–21. https://doi.org/10.2214/AJR.20.23219.
20. Alabousi M, Salameh J-P, Gusenbauer K, Samoilov L, Jafri A, Yu H, et al. Biparametric vs multiparametric prostate magnetic resonance imaging for the detection of prostate cancer in treatment-naïve patients: a diagnostic test accuracy systematic review and meta-analysis. BJU Int. 2019. https://doi.org/10.1111/bju.14759.
21. DeLong ER, DeLong DM, Clarke-Pearson DL. Comparing the areas under two or more correlated receiver operating characteristic curves: a nonparametric approach. Biometrics. 1988;44:837–45.
22. Kerr KF, Brown MD, Zhu K, Janes H. Assessing the clinical impact of risk prediction models with decision curves: guidance for correct interpretation and appropriate use. J Clin Oncol Off J Am Soc Clin Oncol. 2016;34:2534–40. https://doi.org/10.1200/JCO.2015.65.5654.
23. Van Calster B, Nieboer D, Vergouwe Y, De Cock B, Pencina MJ, Steyerberg EW. A calibration hierarchy for risk models was defined: from utopia to empirical data. J Clin Epidemiol. 2016;74:167–76. https://doi.org/10.1016/j.jclinepi.2015.12.005.
24. Brancato V, Aiello M, Basso L, Monti S, Palumbo L, Di Costanzo G, et al. Evaluation of a multiparametric MRI radiomic-based approach for stratification of equivocal PI-RADS 3 and upgraded PI-RADS 4 prostatic lesions. Sci Rep. 2021;11:643. https://doi.org/10.1038/s41598-020-80749-5.
25. Corsi A, De Bernardi E, Bonaffini PA, Franco PN, Nicoletta D, Simonini R, et al. Radiomics in PI-RADS 3 multiparametric MRI for prostate cancer identification: literature models Re-Implementation and proposal of a Clinical-Radiological model. J Clin Med. 2022;11:6304. https://doi.org/10.3390/jcm11216304.
26. Giambelluca D, Cannella R, Vernuccio F, Comelli A, Pavone A, Salvaggio L, et al. PI-RADS 3 lesions: role of prostate MRI texture analysis in the identification of prostate cancer. Curr Probl Diagn Radiol. 2021;50:175–85. https://doi.org/10.1067/j.cpradiol.2019.10.009.
27. Hectors SJ, Cherny M, Yadav KK, Beksaç AT, Thulasidass H, Lewis S, et al. Radiomics features measured with multiparametric magnetic resonance imaging predict prostate cancer aggressiveness. J Urol. 2019;202:498–505. https://doi.org/10.1097/JU.0000000000000272.
28. Hou Y, Bao M-L, Wu C-J, Zhang J, Zhang Y-D, Shi H-B. A radiomics machine learning-based redefining score robustly identifies clinically significant prostate cancer in equivocal PI-RADS score 3 lesions. Abdom Radiol N Y. 2020;45:4223–34. https://doi.org/10.1007/s00261-020-02678-1.
29. Jin P, Yang L, Qiao X, Hu C, Hu C, Wang X, et al. Utility of Clinical-Radiomic model to identify clinically significant prostate cancer in biparametric MRI PI-RADS V2.1 category 3 lesions. Front Oncol. 2022;12:840786. https://doi.org/10.3389/fonc.2022.840786.
30. Lim CS, Abreu-Gomez J, Thornhill R, James N, Al Kindi A, Lim AS, et al. Utility of machine learning of apparent diffusion coefficient (ADC) and T2-weighted (T2W) radiomic features in PI-RADS version 2.1 category 3 lesions to predict prostate cancer diagnosis. Abdom Radiol. 2021;46:5647–58. https://doi.org/10.1007/s00261-021-03235-0.
31. Nketiah G, Elschot M, Kim E, Teruel JR, Scheenen TW, Bathen TF, et al. T2-weighted MRI-derived textural features reflect prostate cancer aggressiveness: preliminary results. Eur Radiol. 2017;27:3050–9. https://doi.org/10.1007/s00330-016-4663-1.

32. Chawla NV, Bowyer KW, Hall LO, Kegelmeyer WP. SMOTE: synthetic minority Over-sampling technique. J Artif Intell Res. 2002;16:321–57. https://doi.org/10.1613/jair.953.
33. Losnegård A, Reisæter LAR, Halvorsen OJ, Jurek J, Assmus J, Arnes JB, et al. Magnetic resonance radiomics for prediction of extraprostatic extension in non-favorable intermediate- and high-risk prostate cancer patients. Acta Radiol. 2020;61:1570–9. https://doi.org/10.1177/0284185120905066.

Publisher's note